Methanol Conversion to Hydrocarbons (MTH) Over H-ITQ-13 (ITH) Zeolite

Supporting information

Methanol conversion to Hydrocarbons (MTH) over H-ITQ-13 (ITH) zeolite

Wegard Skistad[a], Shewangizaw Teketel[a], Francesca Lønstad Bleken[a], Pablo Beato[b], Silvia Bordiga[a,c], Merete Hellner Nilsen[a], Unni Olsbye[a], Stian Svelle[a,] and Karl Petter Lillerud[a]*

[a]inGAP Center for Research Based Innovation, Department of Chemistry, University of Oslo, P.O.Box 1033 Blindern, N-0315 Oslo, Norway.

[b]Haldor Topsøe, Nymøllevej 55, DK-2800 Kgs. Lyngby, Denmark

[c]Department of Chemistry, INSTM Centro di Riferimento and NIS Centre of Excellence Universita' di Torino, Via Quarello 15, 10135 Torino, Italy

*Corresponding author: stian.svelle@kjemi.uio.no

Fax: +47 22 85 54 41

Tel: +47 22 85 54 54

Contents

S.1 XRD, SEM, Sorption measurements and FTIR

S.1.1 XRD

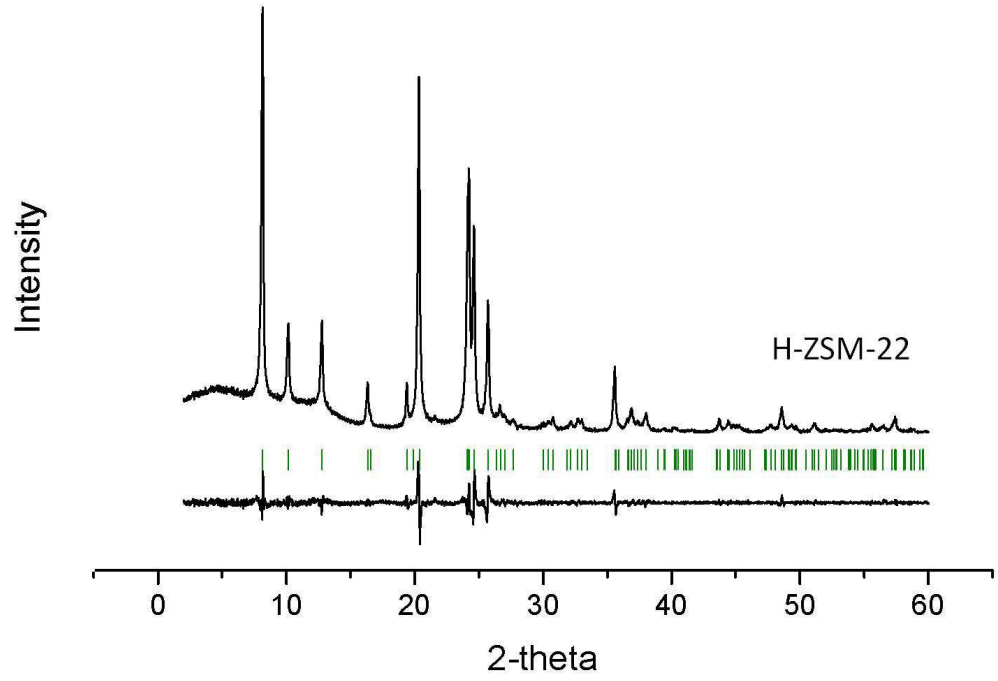

Figure S 1: X-ray diffractogram (XRD) of H-ZSM-22. Bars represent theoretical peak positions and the profile represents the difference between simulated and experimental diffraction patterns (Pawley-refinement). Similar experimental conditions as stated in the main article section 2.2 was followed.

The ZSM-5, PZ-2/100H, sample was supplied from ZeoCat. XRD is not avaliable.

S.1.2 SEM and acid site density

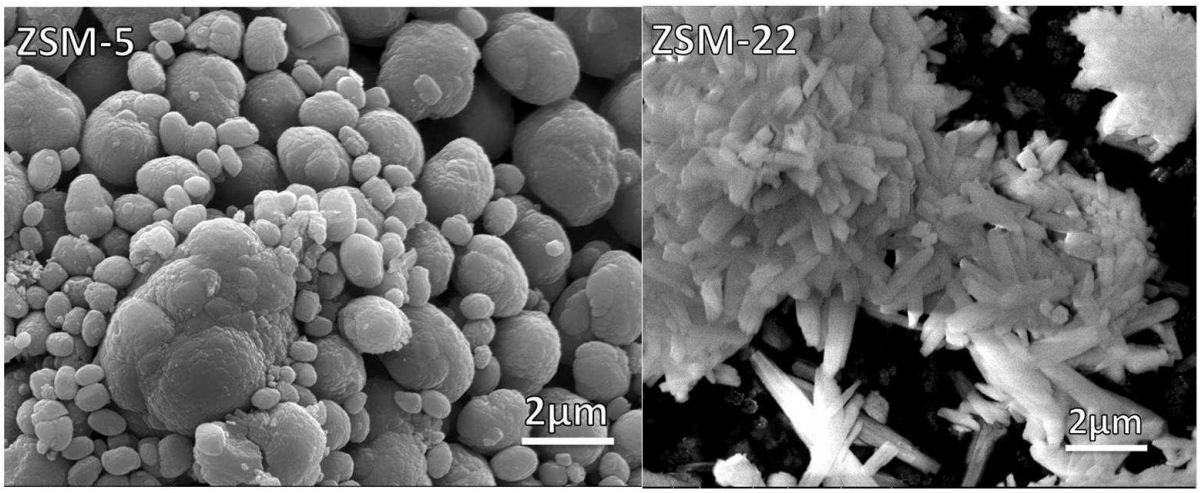

Figure S 2: SEM micrographs of ZSM-5 (left panel) and ZSM-22 (right panel). ZSM-5 had typically (3D) elliptical shape while ZSM-22 was rod-like.

Table S 1: Overview over acid site density and morphology

Morphology and acid site density					
Sample	Si/Al_{EDS}	$Si/Al_{Supplier}$	Si/Al_{TPD}	Particle shape	Particle size
H-ITQ-13 (N)	42	-	N/A	Needles	< 3µm ×100 nm
H-ITQ-13 (P)	>100	-	N/A	Plate-like	Typically 1 µm in the longest direction
H-ZSM-22	N/A	50	48	Rods	Typically 1-3 µm length
H-ZSM-5	49	50	N/A	Elliptical	< 5 µm, typically < 2.5 µm

N/A: Not available

S.1.3 Sorption measurements

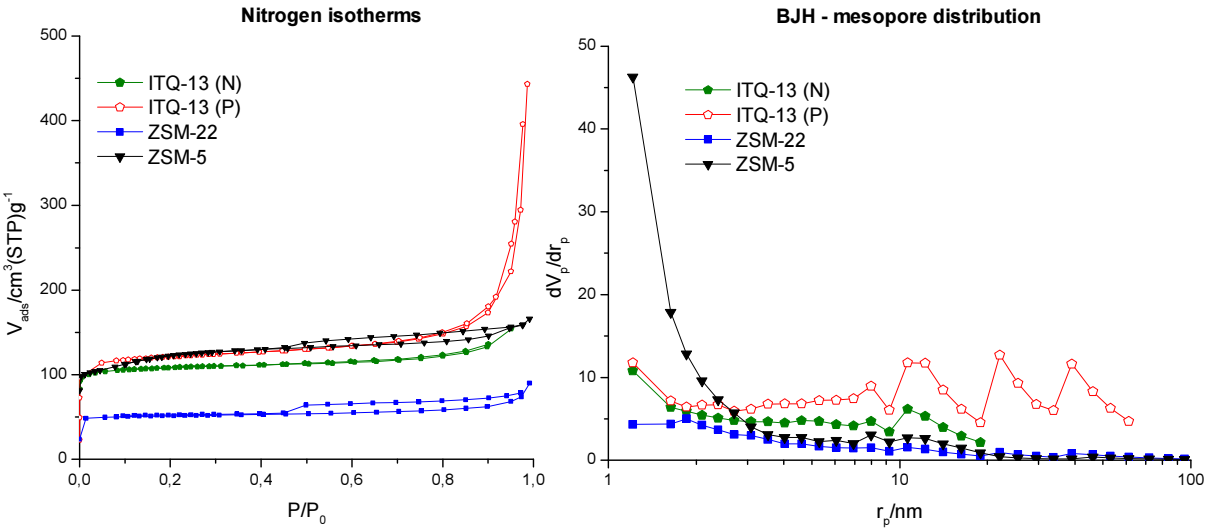

Figure S 3: Nitrogen sorption isotherms of H-ITQ-13 (N) and (P), H-ZSM-22 and H-ZSM-5 are shown in the left panel. The corresponding mesopore distribution plots are shown in the right panel. H-ZSM-5 and H-ZSM-22 showed a small hystersis curve which is likely due to intercrystalline voids.

Table S 2: Nitrogen physisorption data at liquid N_2 temperature

Nitrogen sorption measurements						
Sample	S_{BET} (m^2/g)	S_{ext} (m^2/g)	S_{Micro} (m^2/g)	V_{Total} (cm^3/g)[h]	V_{Micro} (cm^3/g)	V_{Meso} (cm^2/g)
H-ITQ-13 (N)	413	45	368	0.24	0.15	0.09
H-ITQ-13 (P)	455	90	365	0.69	0.15	0.54
H-ZSM-22	197	20	178	0.14	0.07	0.07
H-ZSM-5	430	52	378	0.26	0.16	0.10

S.1.4 FTIR

Table S 3: OH-shift upon CO adsorption

Shift in wavenumber upon CO adsorption				
Sample	Brønsted			Comment
	Without CO [cm^{-1}]	CO adsorption [cm^{-1}]	Shift [Δcm^{-1}]	
H-ITQ-13 (N)	3627 (3610)	3300	-327 (-310)	
H-ITQ-13 (P)	-3627*	3300	-327*	*Uncertain assignement. Brønsted-band barely visible
H-ZSM-22	3600	3284	-316	
H-ZSM-5	3612	3309	-303	

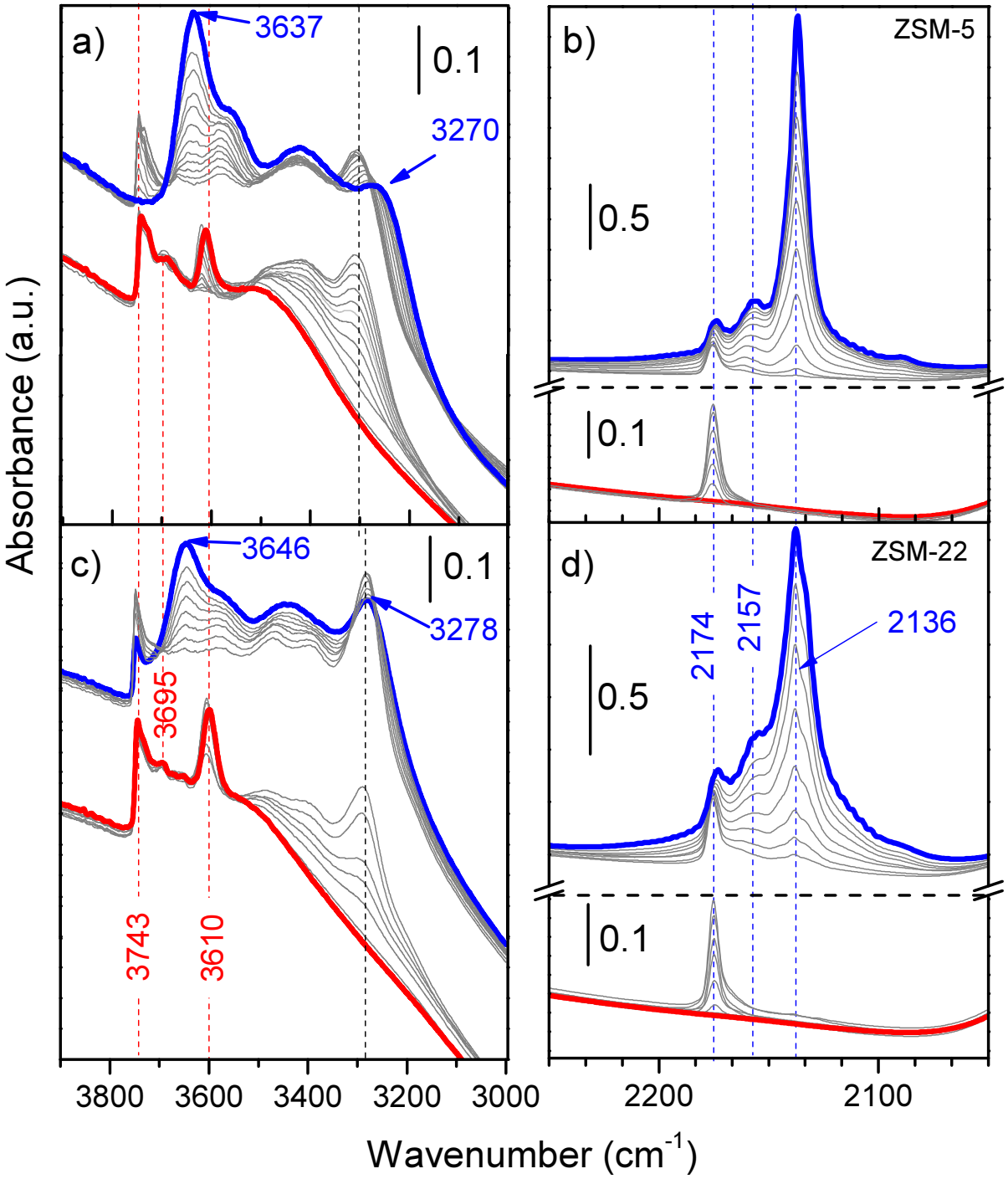

Figure S 4: Infrared spectra of H-ZSM-5 and H-ZSM-22 with increasing CO dose. Red curve shows the zeolite without CO adsorbed and the blue curve shows the maximum CO adsorption. The ν(O-H) region of a) H-ZSM-5 and c) H-ZSM-22 is shown in the left panel while the ν(CO) region of b) H-ZSM-5 and d) H-ZSM-22 is shown to the right

H-ZSM-5 and H-ZSM-22 catalysts were investigated using FTIR spectroscopy measurements displayed in Figure S4. Panels a and b display the OH and CO vibration regions respectively over H-ZSM-5. The IR spectra of the activated H-ZSM-5 zeolites without the probe molecule CO is presented by the red curve. In the OH stretching region (panel a) two bands at 3743 and 3610 cm^{-1} associated with silanols and Brønsted acid site respectively were observed. When CO was added in excess (blue curve), the position of the bands was shifted to lower frequencies. The gray curves display intermediate CO coverages. At maximum coverage, the bands associated with silanols and Brønsted acid site shifted to 3637 and 3270 cm^{-1} (maximum loading) respectively. Such shift of Brønsted band position due to the interaction with probe molecules is a measure of the strength of the acid sites.

Similarly, the results over ZSM-22 are displayed in panels c and d. The observed frequency shift when adsorbing CO over ZSM-22 and ZSM-5 catalysts (-308 cm^{-1} 303cm^{-1}, respectively) were almost identical, suggesting only slight differences in acid site strength between the two materials. (Note that the shift was calculated where the band is vertically stabilised marked with a dotted line in Figure S 4 and not from the maximum CO-loading) indicating similar acid strength

IR bands were visible in the region 3700 cm^{-1} to ~3650 cm^{-1} were observed in the activated version of both H-ZSM-22 and H-ZSM-5. Such bands are often ascribed to extraframework and/or perturbed framework aluminum atoms. [1] Also, after exposure to CO, the broad band with a maximum (blue curve) around 3435 cm^{-1} (H-ZSM-22) and 3425 cm^{-1} (H-ZSM-5) represents defective sites in interaction with the probe molecule. From FTIR data obtained from H-ITQ-13 in Figure 5 (main article) it was clear that all three materials contained the described defective sites. As described in [1] real evidence of the structure of such defective sites is not straightforward and several mechanisms can be possible. Perturbed aluminum atoms can be formed via a stepwise weakening of the Al-OH in Si-(OH)-Al with formation of Si-OH groups. The trigonal Al atom is not stable and can be partly removed from the zeolite framework by terminal Al-OH groups[1]. In addition Lewis-sites can be formed by dehydroxylation reactions combining a terminal OH group with a proton from another group. This implies that many possible defective sites involving aluminium can be formed.

S.2 Conversion versus TOS

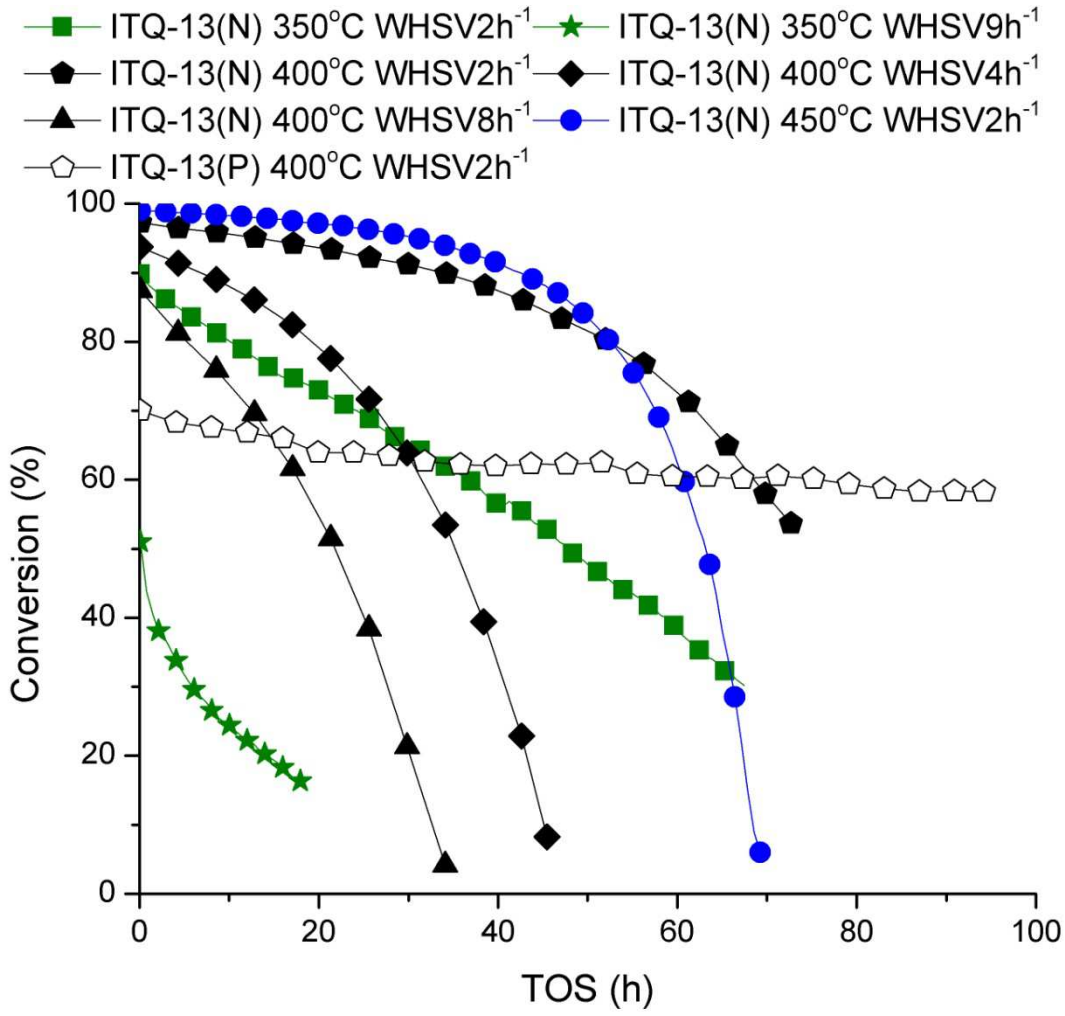

Figure S5: Conversion versus time on stream (TOS) at different temperatures (350˚C-450˚C) and WHSV in the range of 2-9 h^{-1} for H- ITQ-13

Figure S5 summarizes the effects of temperature and contact time (feed rate) on the deactivation profile of H-ITQ-13. At 450˚C and WHSV = 2 h^{-1}, near full methanol conversion was observed over the fresh catalyst and slight deactivation was observed after several hours on stream. Slightly lower conversion (97 %) was observed at 400˚C for the same feed rate, while at 350˚C the initial conversion dropped to 90 %. A close to linear decrease of the conversion (constant slope) was observed for the latter while at 400 and 450˚C slower deactivation took place until ~50h on stream followed by a relatively rapid deactivation of the catalyst. The effect of feed rate on the lifetime of the catalyst was investigated at 350 (green curves) and 400 °C (black curves). At 350˚C and WHSV = $9h^{-1}$ the initial conversion was only slightly above 50% and rapidly decreased with time on stream, while WHSV = $2h^{-1}$ the initial methanol conversion was ~90%. Similarly at 400 °C, a decrease in the lifetime of the catalysts and initial methanol conversion over the fresh catalyst was observed with

increasing feed rate (WHSV). The life-time cycle of MTH catalysts has been addressed in several recent contributions [2-4]. It has been found that for catalysts with less than 100 % initial conversion, the initial slope of the conversion versus time on stream curve represents the sum of simultaneous creation and loss of active sites [3, 4]. Therefore, catalyst stability cannot be read from such plots alone, but rather from comparing the total methanol conversion capacity of each catalyst under a given set of conditions [4].

S.3 Total conversion capacity

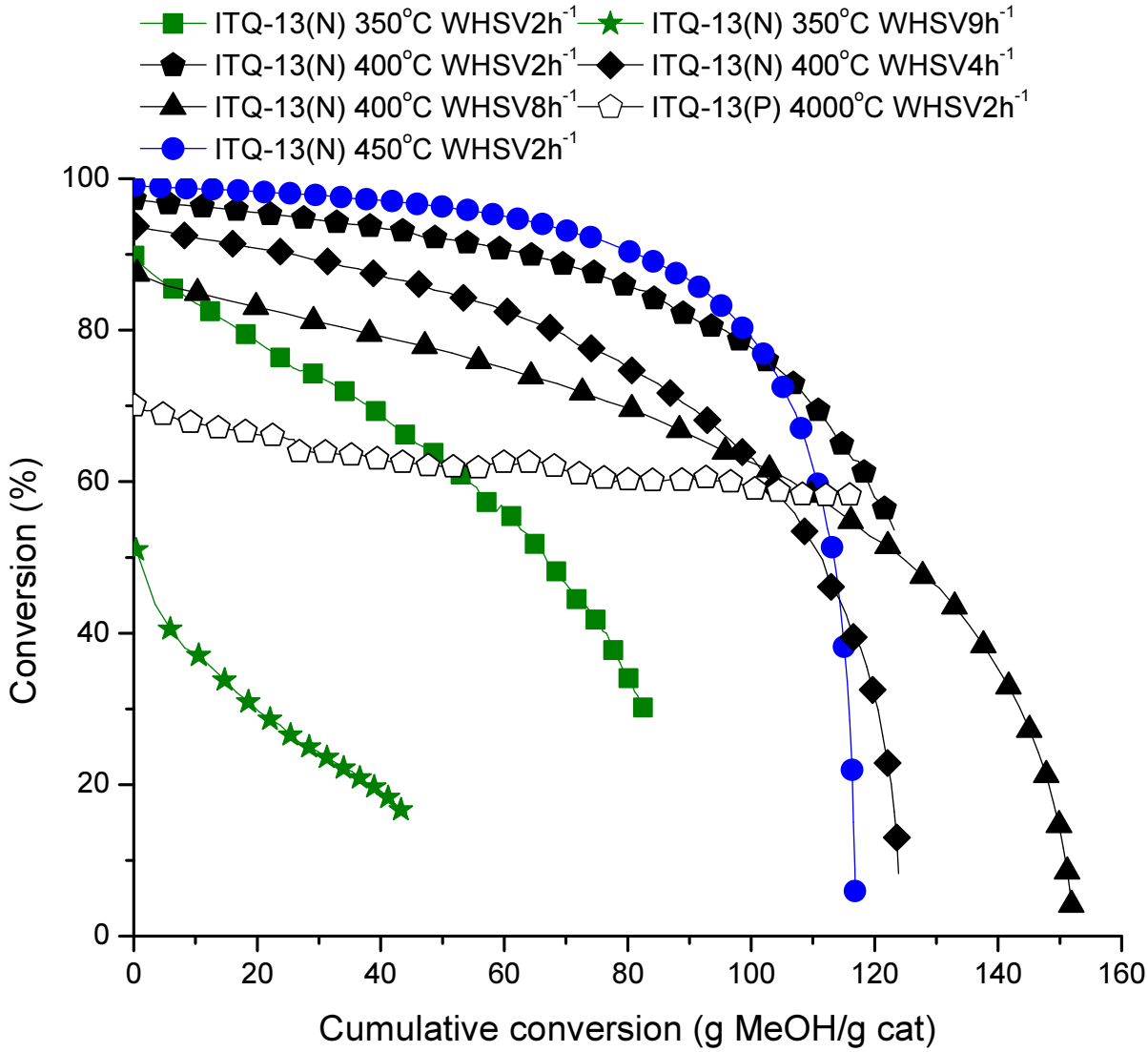

Figure S6: Cumulative conversion at different reaction conditions.

Figure S6 shows the total conversion capacity, defined as the amount (in grams) of methanol converted to products per gram of catalyst over H-ITQ-13 (N) under various conditions. The lowest conversion capacity was observed at the lowest temperature 350˚C and WHSV = $2h^{-1}$, which displayed a total conversion capacity of ~100 g methanol per gram of catalyst. An increase in the

total conversion capacity was observed with increasing reaction temperature from 350 °C to 400 and 450 °C, which resulted in the total conversion capacities in the range 118-152 gram methanol converted per gram catalyst. It is interesting to note that the total conversion capacities at 400 and 450 °C were comparable. The deactivation of H-ITQ-13(P) was slow and despite the low initial conversion (and no clear indication of a rapid change in conversion versus TOS or cumulative conversion) the total conversion capacity was likely to exceed all results obtained over the H-ITQ-13 (N) sample.

As seen from Figure S6, feed rate (WHSV) had a minor effect on the total conversion capacity over H-ITQ-13(N). The different feed rates at 400 °C (WHSV = 2-8 h^{-1}) displayed total conversion capacities in the range 125-152 gram methanol converted per gram catalyst. Similarly, at 350 °C the total conversion capacity, allowing extrapolation of the graphs, was in the range of 70-100 g methanol per gram of catalyst.

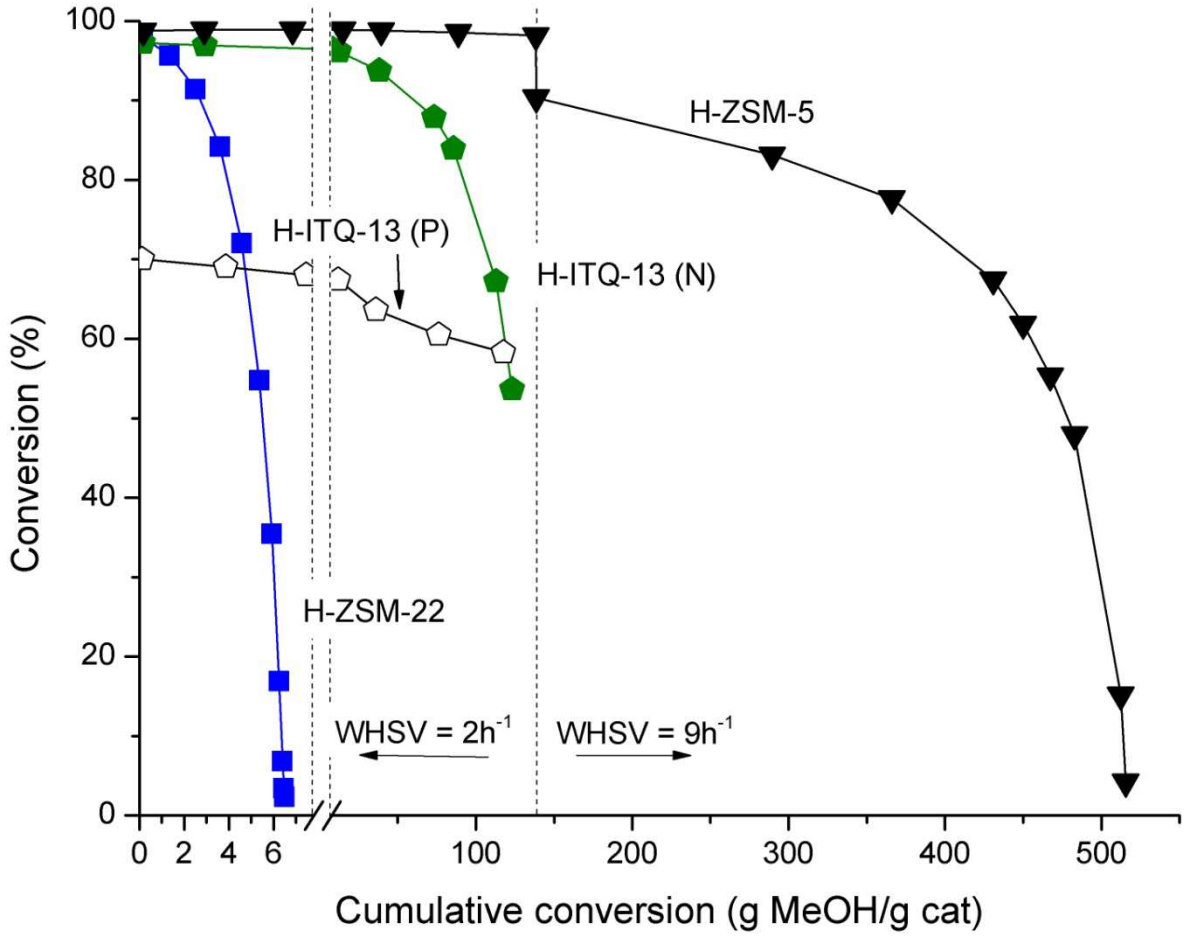

Figure S7 Cumulative conversion over H-ZSM-22, H-ITQ-13 (N) and (P) and H-ZSM-5. The drop in conversion observed for H-ZSM-5 (triangels) is caused by a change in the WHSV from $2h^{-1}$ to $9h^{-1}$. Else all the reactions were carried out at 400˚C and WHSV = $2h^{-1}$.

Figure S7 shows the cumulative methanol conversion over H-ITQ-13(N), H-ITQ-13(P), H-ZSM-5 and H-ZSM-22 at 400˚C and WHSV = $2h^{-1}$ except for the change from 2 to 9 h^{-1} for H-ZSM-5 to let the material deactivate. The total conversion capacity of H-ZSM-22 was 6.5 g methanol per gram of catalyst (it should be noted that a plot of time to 50 % dectivation versus initial contact time for this H-ZSM-22 sample under the conditions reported here gave a slightly higher total conversion capacity of 9.9 g methanol per gram of catalyst [4]), while ~520 g methanol per gram of catalyst could be converted over H-ZSM-5. Allowing extrapolation of the H-ITQ-13(N) curve the total conversion capacity was ~140 g methanol per gram of catalyst. The H-ITQ-13 (P) sample showed no clear change in the conversion and thus it was not possible to state a total conversion capacity for this sample. However it is very likely to boost the results obtained for H-ITQ-13 (N) as described above. From these results the total conversion capacity H-ITQ-13(N) falls in between the one-dimensional H-ZSM-22 and the tri-dimensional H-ZSM-5, yet closer to H-ZSM-5.

S.4 Product yield versus conversion

Figure S8 shows yields as a function of conversion for methane, C_2 and C_3, C_4 alkenes and C_4 alkanes, C_5, and C_6^+ aliphatics and aromatics with onset of reaction at right (high conversion) with time evolution towards the left (low conversion) side at different temperatures and WHSV.

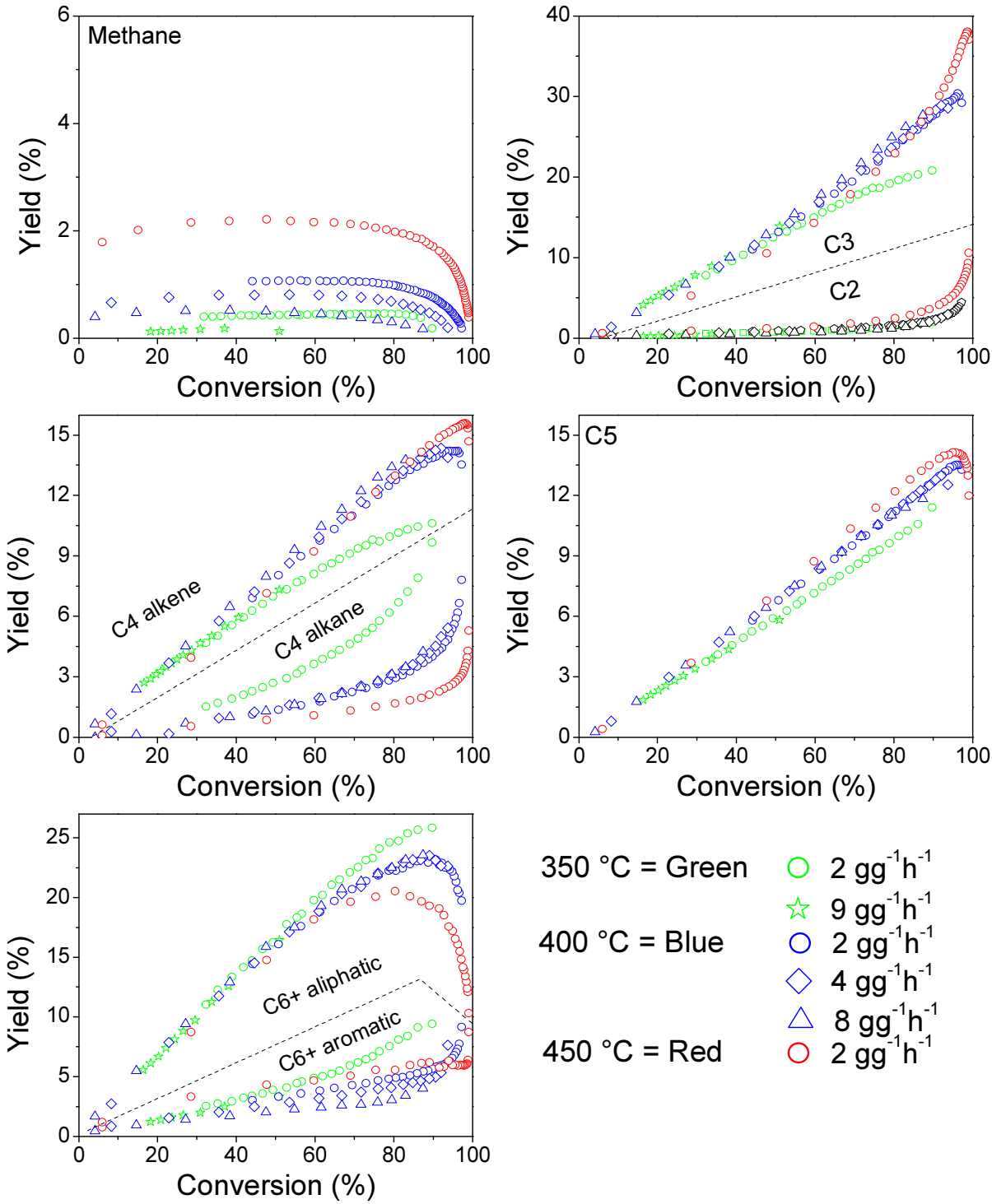

Figure S8: Product yield as a function of conversion obtained over H-ITQ-13 (N) at different temperatures and at WHSV = 2-9h^{-1}.

For a wide range of conversions (~15-96%) C_3 and C_6^+ aliphatics were the dominating product fractions in MTH over H-ITQ-13(N). At the highest conversion points at 450˚C the yield of C_6^+ aliphatics was low, lower than the yield of the C_4 alkene and C_5 fraction. However a rapid increase towards ~ 96% conversion was observed. The ratio between the C_6^+ and the C_3 fractions changed depending on temperature and the extent of deactivation. At 450˚C and 400˚C and high conversions (above 75% and 76 % respectively) the yield was higher for C_3 fractions compared to C_6^+ aliphatics and the situation inverted below these conversions, while at 350˚C more C_6^+ aliphatics than C_3 was formed for all data points collected. Typically the gasoline range is reported as the combined fraction of C_5, C_6^+ aliphatics and C_6^+ aromatics denoted as C_5^+ and together they were the clearly dominating fraction. Here less than 10 % of the total yield was aromatic compounds, predominantly 1,2,4-trimethylbenzene (and xylenes). The effect of temperature on the aromatic contribution was in accordance to thermodynamics which means that more aromatics were present when the temperature was decreased from 450 to 350˚C. However the change in yield as a function of deactivation resulted in curve crossing giving the highest yield of aromatics at 450˚C for the lower conversion side. Since the aromatics at its maximum contributed ~10 % to the total yield, C_5 and the C_6^+ aliphatics (linear and branched alkanes and alkenes) counted for more than 90 % of the gasoline fraction and the C_6^+aliphatics/C_5 -ratio decreased for increasing temperature. (The selectivity towards C_5^+ shown in Figure S9 increased upon deactivation and at 350˚C it was in the range of 51-54 %, 43-51 % at 400˚C and 31-55 % at 450˚C. Thus, roughly 50 % of the product selectivity was denoted to the gasoline range).

The C_4 fraction was divided into C_4 alkenes and C_4 alkanes. At comparable conversions the yield of C_4 alkenes was higher than for the corresponding C_4 alkanes. The ratio between these two fractions changed as a function of temperature. Ranging from low to high temperatures the C_4 alkanes decreased while there was an increase among the C_4 alkenes. This was in accordance with the higher aromatic yield at lower temperatures since those aromatic compounds have a high C/H ratio. Hence the formation of aromatic compounds is accompanied by hydrogen transfer and thus an increased yield of C_4 alkanes as the temperature was lowered.

In the C_1 and C_2 fraction a higher yield was observed for increased temperature.

The main conclusion drawn from such yield as a function of conversion at different space velocities is described in the main article and in Figure S11 below. As seen from Figure S8, the yield of the various hydrocarbons is clearly dependent on reaction temperature. At high methanol conversion variation (> 90%), a systematic increase in the yield of light hydrocarbons with increasing temperature is observed, and it is clearly visible for C_3 and C_4 alkene. This could be ascribed to cracking reactions which are favored at high temperatures. On the other hand, low reaction temperature favors the

formation of relatively higher hydrocarbons, which is visible for C_{6+} aliphatic, C_{6+} aromatic and C_4 alkanes (which is linked to the formation of aromatic hydrocarbons). The formation of methane is generally linked to formation of heavy coke species which are not detected in the gas phase effluent. Hence, the formation of relatively higher amounts of methane with increasing reaction temperature could be an indication of enhanced coke formation with temperature, and this could be the reason for the high negative slope of the conversion versus time on stream curves at the higher reaction temperatures shown in Figure S5.

S5 Selectivity

S5.1 The effect of temperature

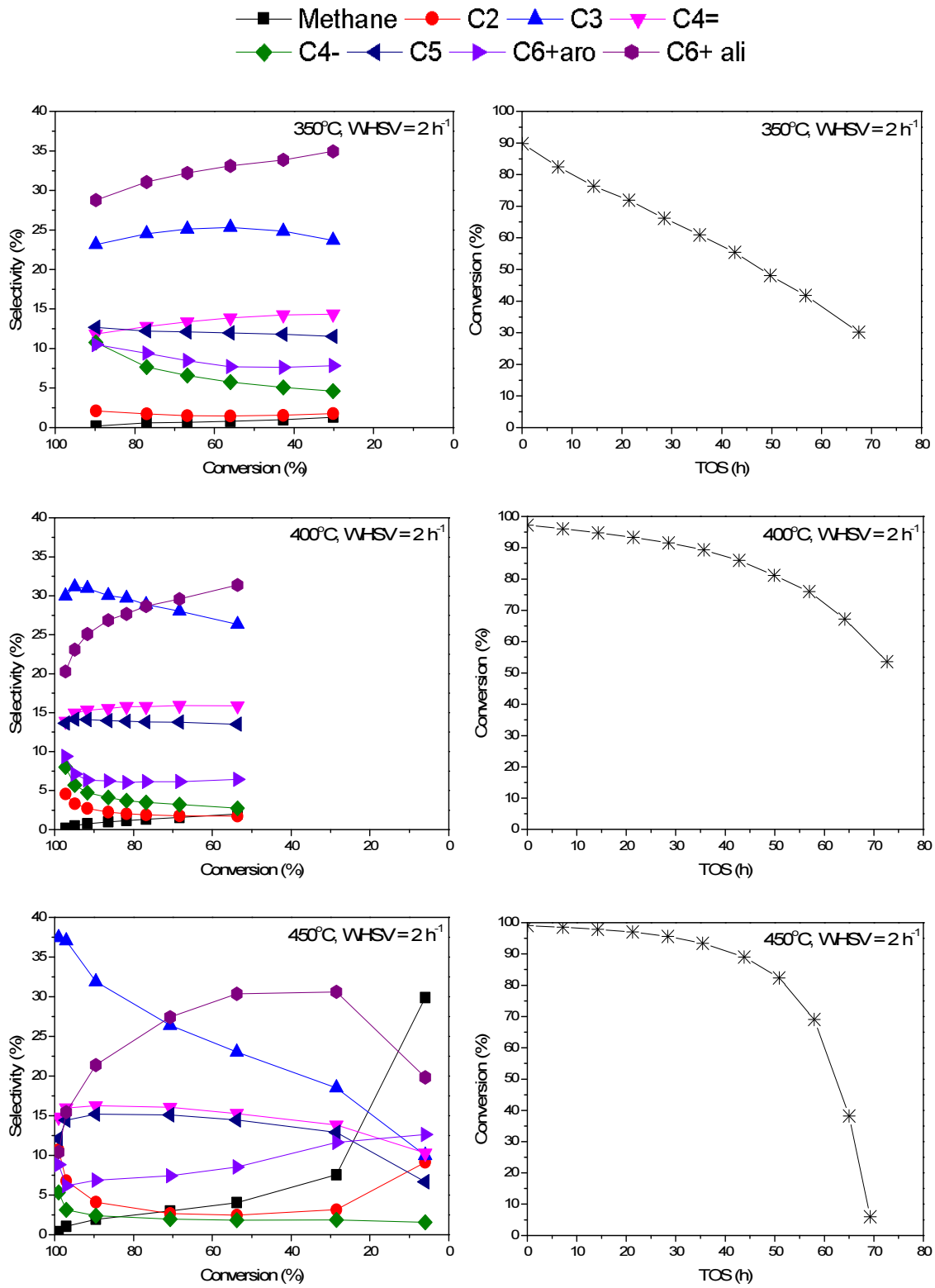

Figure S9: Selectivities obtained from H-ITQ-13 (N) as a function of conversion at different temperatures is given in the left panels. The corresponding Conversion vs TOS is shown in right panels.

S5.2 The effect of change in WHSV

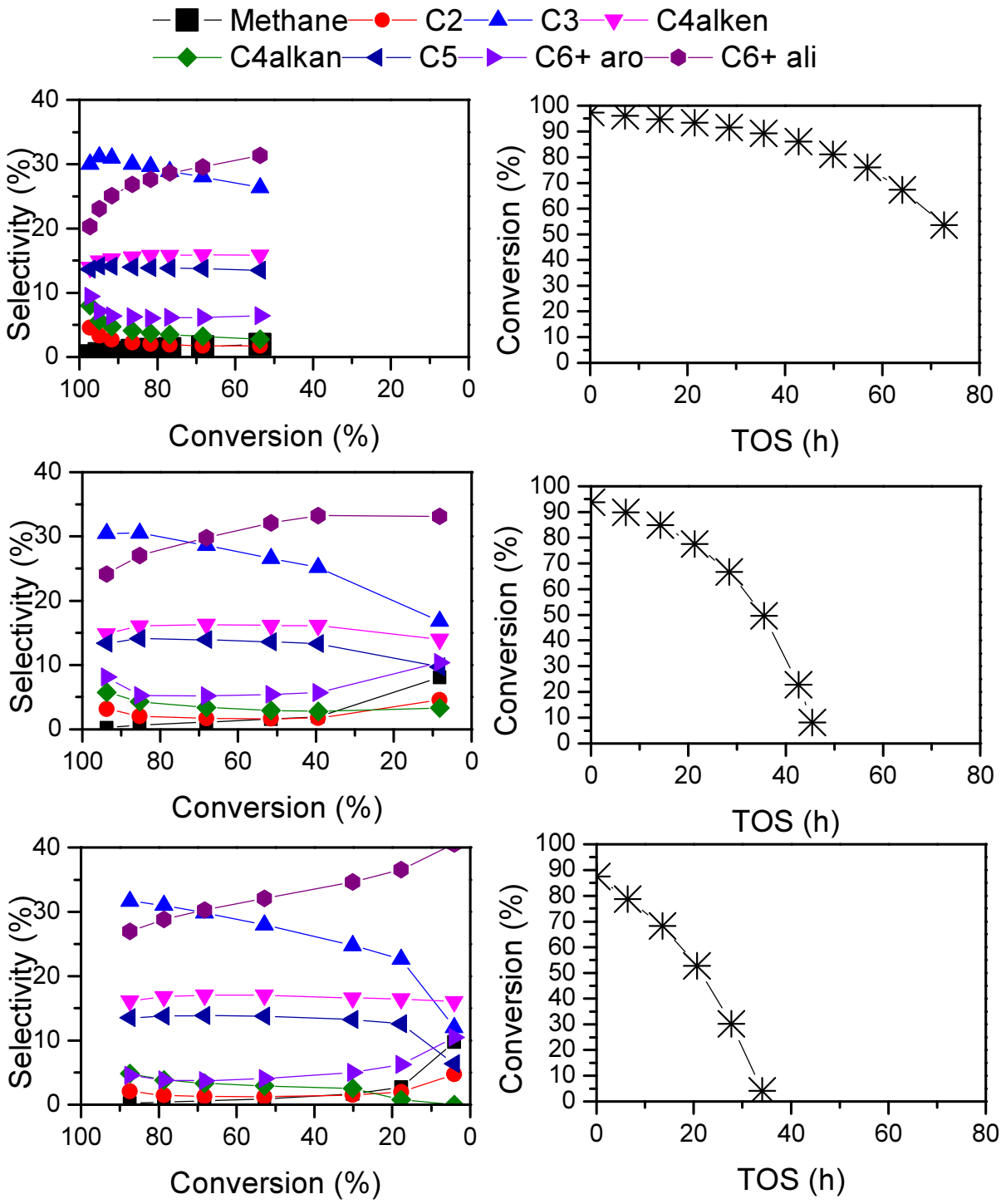

Figure S10: Selectivity versus conversion obtained over H-ITQ-13 (N) at 400˚C when the WHSV ranged from 2-8h^{-1} . Corresponding graphs showing conversion versus TOS (h) are shown in the right panels. Top panels: 400˚C, WHSV = 2 h^{-1}, Mid panels: 400˚C, WHSV = 4 h^{-1} and bottum panels: 400˚C, WHSV = 8 h^{-1}.

S.6 The effect of deactivation on selectivity

Figure S11 shows the yield as a function of conversion at 350 °C and corresponds to the graph in the main article describing the effect of deactivation on selectivity at 400 °C. The sample at WHSV = $2h^{-1}$ had been ~62h on stream before achieving the same conversion as the initial conversion of the sample at WHSV = $9h^{-1}$. The conclusion of non-selective deactivation is in agreement with the results published in the main article at 400˚C and WHSV = 2, 4 and $8h^{-1}$.

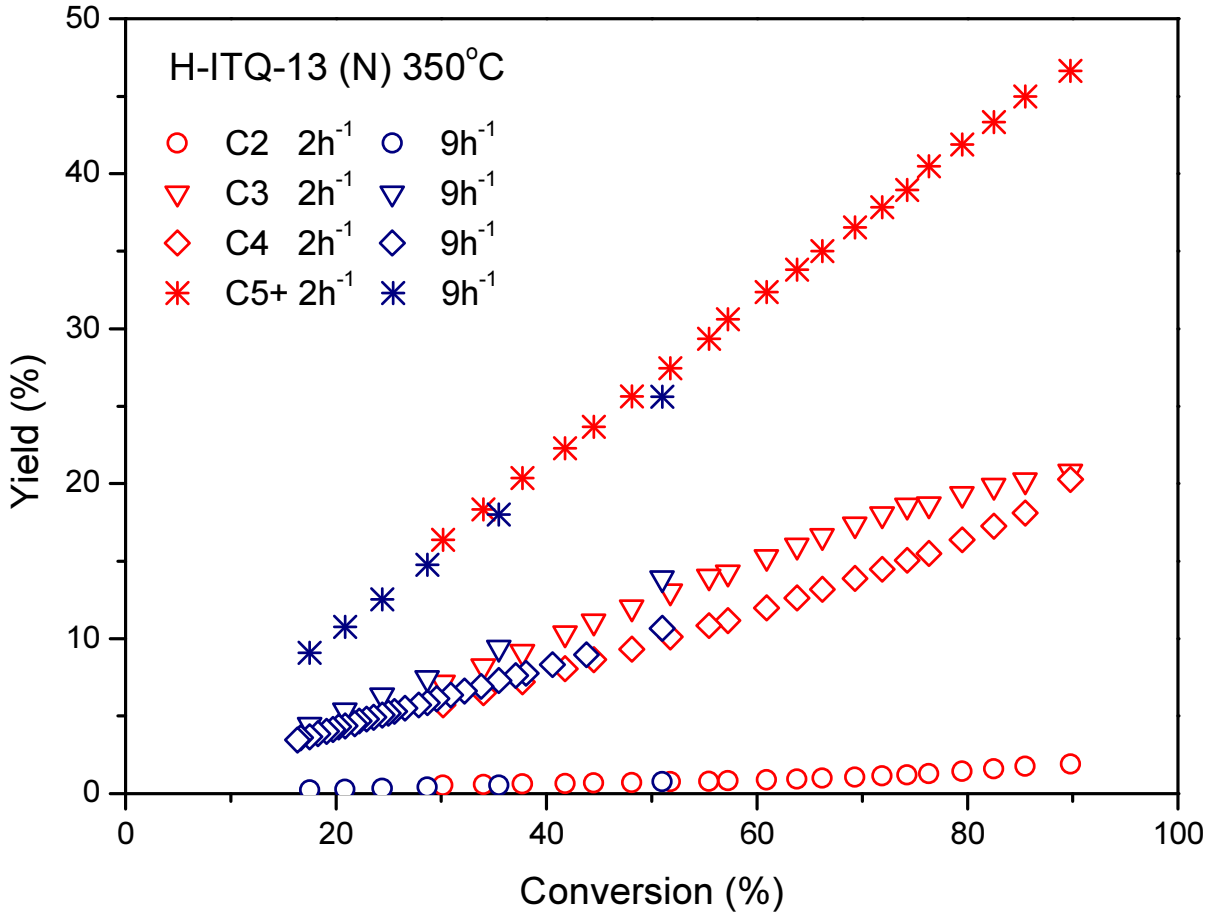

Figure S11: The effect of deactivation on selectivity over H-ITQ-13(N) at 350˚C and WHSV = $2h^{-1}$ and $9h^{-1}$.

References

[1] M. Milina, S. Mitchell, Z.D. Trinidad, D. Verboekend, J. Perez-Ramirez, Catal. Sci. Technol. 2 (2012) 759-766.

[2] T.V.W. Janssens, J. Catal. 264 (2009) 130-137.

[3] D.S. Wragg, M.G.O. Brien, F.L. Bleken, M. Di Michiel, U. Olsbye, H. Fjellvag, Angew. Chem. Int. Edit. 51 (2012) 7956-7959.
[4] T.V.W. Janssens, S. Svelle, U. Olsbye, J. Catal. (2013) Accepted.